Int. J. Appl. Math. Comput. Sci., 2024, Vol. 34, No. 4, 549–563
DOI: 10.61822/amcs-2024-0037

OPTIMIZING INFECTIOUS DISEASE DIAGNOSTICS THROUGH AI–DRIVEN HYBRID DECISION MAKING STRUCTURES BASED ON IMAGE ANALYSIS

MUHAMMAD AHSAN [a], ROBERTAS DAMAŠEVIČIUS [a,*], SARMAD SHAHZAD [b]

[a]Faculty of Informatics
Vytautas Magnus University
28, K. Donelaičio, 44246 Kaunas, Lithuania
e-mail: ahsan1826@gmail.com, robertas.damasevicius@vdu.lt

[b]Department of Mathematics
Riphah International University
1, Main Satiana Road, 38000 Faisalabad, Punjab, Pakistan
e-mail: sarmad923@gmail.com

Infectious diseases significantly impact global mortality rates, with their complex symptoms complicating the assessment and determination of infection severity. Various countries grapple with different forms of these diseases. This research utilizes three AI-based decision-making techniques to refine diagnostic processes through the analysis of medical imagery. The goal is achieved by developing a mathematical model that identifies potential infectious diseases from medical images, adopting a multi-criteria decision-making approach. The avant-garde, AI-centric methodologies are introduced, harnessing an innovative amalgamation of hypersoft sets in a fuzzy context. Decision-making might include recommendations for isolation, quarantine in domestic or specialized environments, or hospital admission for treatment. Visual representations are used to enhance comprehension and underscore the importance and efficacy of the proposed method. The foundational theory and outcomes associated with this innovative approach indicate its potential for broad application in areas like machine learning, deep learning, and pattern recognition.

Keywords: medical imaging, fuzzy logic, disease diagnostics, decision support, health informatics.

1. Introduction

Infectious diseases pose a serious threat to global health, causing millions of deaths each year and affecting people of all ages and geographies. These diseases are caused by a variety of pathogens, including viruses, bacteria, fungi and insects (Morse, 1995; Fauci and Morens, 2012). Practices such as sanitation, vaccination and drug prevention are critical to controlling these diseases, as is ongoing research to improve these practices. In health care, decision making is essential for proper diagnosis and treatment and requires consideration of many complex factors. The use of technology, especially data analytics tools, has greatly improved the ability to tailor treatment to the needs of the individual patient, thus improving clinical outcomes (Lauraitis *et al*., 2018; Omoregbe *et al*., 2020). To further improve healthcare decision making, HSS (hybrid soft set) theory combines aspects of fuzzy and soft set theories to better handle uncertainty and imprecise data in healthcare environments. This paper presents an innovative application of artificial intelligence-based tools using HSSs in a trivial framework for medical image analysis. The framework, incorporating a multi-criteria decision model (MCDM), aims to improve infectious disease detection by leveraging the power of machine learning, deep learning and pattern recognition to optimize decision-making processes in the field life.

1.1. Related works. Artificial intelligence (AI) has significantly shaped the evolution of healthcare practices over the years. Initially, AI's integration focused on administrative tasks such as tracking medical histories efficiently, a foundational step that was instrumental for later advancements in the field. Davenport *et al*. (2018)

*Corresponding author

highlighted this early application of AI in healthcare. By 2020, the scope of AI expanded to include the translation of clinical information, facilitating better communication between healthcare providers and patients, a development emphasized by Lin and Lin (2020).

Following these early implementations, AI began to play a more significant role in managing healthcare logistics. Curtis *et al*. (2018) documented AI's role in scheduling and administrative logistics, marking a shift towards automating routine tasks within healthcare facilities. By 2023, Vemuri discussed how AI technologies were being utilized for predictive analytics and decision support systems to enhance diagnosis and treatment planning, analyzing both structured and unstructured data such as electronic medical records and medical images (Vemuri, 2023; Vemuri *et al.*, 2023b; 2023a).

The capabilities of AI continued to evolve, and Hasan *et al*. (2024) and Ray *et al*. (2024) explored how AI techniques like machine learning and deep learning were used to analyze healthcare data to identify trends that may be overlooked by human analysts, thereby improving diagnostics and treatment outcomes. This progression demonstrates AI's transition from enhancing administrative efficiency to playing a pivotal role in clinical decision-making.

However, certain challenges remained, such as accurately processing medical images under poor lighting conditions. Traditional techniques like gray-level modifications were found inadequate (Ramu and Bansal, 2024). In response, by 2023, new methodologies employing fuzzy sets and intuitionistic fuzzy sets (IFSs) were developed to improve uncertainty management in image processing, which facilitated more precise disease diagnoses (Zadeh, 1965; Atanassov, 2012). Technologies like the fuzzy DBNet, integrating fuzzy techniques with deep learning, achieved high segmentation accuracy, surpassing previous methods (Chin *et al*., 2023; Nagaraja Kumar *et al*., 2023).

Furthermore, AI application in forecasting and managing disease outbreaks has been critical. Sundus *et al.* (2024) emphasized AI's utility in analyzing vast datasets to predict disease outbreaks, which is vital for the proactive management of health crises. In 2024, a survey of healthcare executives in the United States reaffirmed AI's essential role in promoting health equity, reflecting its increasing importance in addressing broader healthcare challenges (Mumuni *et al*., 2024). These developments underscore AI's fundamental role in not only advancing healthcare operations and patient care but also in tackling global health issues.

1.2. Motivation/research gap. The primary objective of this study is to create a model that employs artificial intelligence techniques, with a special emphasis on incorporating hypersoft sets (HSSs) within a fuzzy framework, aimed at improving the analysis of images for infectious diseases. This model is vital for providing accurate recommendations for isolation, quarantine, or hospitalization, thereby facilitating effective treatment. Existing theories and methods struggle with the precise identification and application of medical imaging for diagnostics, a challenge highlighted by Chaira (2011), Koundal and Sharma (2019), Kaur and Chaira (2021) or Dey *et al*. (2018). These traditional approaches are inadequate for developing comprehensive models capable of addressing the complexities and dynamic nature of infectious diseases.

In particular, the methodologies outlined by Kaur and Chaira (2021) and Dey *et al*. (2018) are ineffective for the proposed model for two primary reasons: they fail to tackle the problems associated with the presence of non-membership (false) elements in data, and they are incapable of efficiently processing information in a sub-parametric form, which is essential for a thorough understanding and appropriate treatment of diseases. Meanwhile, the models introduced by Chaira (2011) and Koundal and Sharma (2019) struggle with managing data characterized by sub-parametric values. This research aims to overcome these shortcomings by suggesting a hybrid model that merges the advantages of HSSs with the ability to delve into disease analysis through sub-parametric values. This advanced model is adept at navigating the complexities of data, including false elements and the subtle, sub-parametric aspects of information, which are frequently neglected in conventional diagnoses. Consequently, it significantly improves the precision of treatment recommendations, encompassing decisions regarding isolation, quarantine, and hospitalization. This study not only narrows the gap between symptoms and treatments, simplifying the decision-making process, but also sets a strong foundation for scientific modeling in the field of medical diagnosis through AI-enhanced decision-making.

2. Methodologies

Definition 1. (*Kamacı, 2021*) Let us define the universe of discourse as

$$\mathfrak{X} = \{\alpha_1, \alpha_2, \alpha_3, \ldots, \alpha_{\mathfrak{n}}\},$$

where α_j for $j = 1, 2, \ldots, \mathfrak{n}$ represents the elements of the universe. We consider $\mathfrak{m}$ distinct attributes denoted by

$$\epsilon_1, \epsilon_2, \epsilon_3, \ldots, \epsilon_{\mathfrak{m}},$$

where ϵ_i for $i = 1, 2, \ldots, \mathfrak{m}$ and $\mathfrak{m} \geq 1$. The characteristic values corresponding to these attributes are

represented by the sets

$$\eth_1, \eth_2, \eth_3, \ldots, \eth_{\mathfrak{m}}.$$

Introduce a function

$$\mathfrak{H} : \eth_1 \times \eth_2 \times \eth_3 \times \ldots \times \eth_{\mathfrak{m}} \to \wp(\mathfrak{X}).$$

Let $\Gamma_{\mathfrak{A}}$ and $\Lambda_{\mathfrak{B}} \in \mathfrak{H}$ be two intuitionistic hypersoft sets (IHSS). The IHSS approximate functions for these are given by

$$\gamma_{\mathfrak{A}}(\epsilon_i) = \{(\alpha, \omega_{\mathfrak{A}}(\alpha), \sigma_{\mathfrak{A}}(\alpha)) : \alpha \in \mathfrak{X}\},$$

$$\lambda_{\mathfrak{B}}(\epsilon_i) = \{(\alpha, \omega_{\mathfrak{B}}(\alpha), \sigma_{\mathfrak{B}}(\alpha)) : \alpha \in \mathfrak{X}\}.$$

The distance between $\Gamma_{\mathfrak{A}}$ and $\Lambda_{\mathfrak{B}}$ for the Hamming distance (HD)is determined as follows:

$$d^s_{\text{IHSS}}(\Gamma_{\mathfrak{A}}, \Lambda_{\mathfrak{B}}) = \frac{1}{2\mathfrak{m}} \sum_{i=1}^{\mathfrak{m}} \sum_{j=1}^{\mathfrak{n}} \left(|\omega_{\mathfrak{A}}(\epsilon_i)(\alpha_j) - \omega_{\mathfrak{B}}(\epsilon_i)(\alpha_j)| + |\sigma_{\mathfrak{A}}(\epsilon_i)(\alpha_j) - \sigma_{\mathfrak{B}}(\epsilon_i)(\alpha_j)|\right). \quad (1)$$

Definition 2. (*Yolcu, 2023*) Given the context of an IHSS defined over a universal set $\mathfrak{U}$, let $\Upsilon_{\mathfrak{A}}$ and $\Psi_{\mathfrak{B}}$ symbolize two such spaces. A similarity measure (SM) between these spaces, facilitated by the application of the Hamming distance (HD), introduces an elegant formulation. The first is given by

$$S'_{\text{IHSS}}(\Upsilon\mathfrak{A}, \Psi_{\mathfrak{B}}) = \frac{1}{1 + d^s_{\text{IHSS}}(\Gamma_{\mathfrak{A}}, \Lambda_{\mathfrak{B}})}. \quad (2)$$

Definition 3. (*Hema* et al., *2023*) The newly introduced plithogenic distance measures (PDMs) comprise the following components:

- plithogenic Hamming distance measure ($d^{\mathcal{R}}_H$),
- normalized plithogenic Hamming distance measure ($d^{\mathcal{R}}_{NH}$),
- plithogenic Euclidean distance measure ($d^{\mathcal{R}}_E$),
- normalized plithogenic Euclidean distance measure ($d^{\mathcal{R}}_{NE}$).

These measures are utilized for calculating the distance between two plithogenic hesitant subtractive sets (PHSSs), denoted as $\mathcal{R}_1$ and $\mathcal{R}_2$. Below, we provide the mathematical formulations and discuss specific components and their roles in the context of these distance measures.

Plithogenic Hamming distance (PHD) measure has the form

$$d^{\mathcal{R}}_H(\mathcal{R}_1, \mathcal{R}_2) = \frac{1}{m} \sum_{i=1}^{m} \sum_{j=1}^{l} \left|d^i_{\mathcal{R}_1}(\delta_j) - d^i_{\mathcal{R}_2}(\delta_j)\right| \times \max\left(c^i_F(\delta_j, \delta_d)\right). \quad (3)$$

Normalized plithogenic Hamming distance (NPHD) measure uses normalization introducing a factor of $1/mn$, accommodating the overall data scale

$$d^{\mathcal{R}}_{NH}(\mathcal{R}_1, \mathcal{R}_2) = \frac{1}{mn} \sum_{i=1}^{m} \sum_{j=1}^{l} \left|d^i_{\mathcal{R}_1}(\delta_j) - d^i_{\mathcal{R}_2}(\delta_j)\right| \times \max\left(c^i_F(\delta_j.\delta_d)\right). \quad (4)$$

Plithogenic Euclidean distance (PED) measure is of the form

$$d^{\mathcal{R}}_E(\mathcal{R}_1, \mathcal{R}_2) = \left[\frac{1}{m} \sum_{i=1}^{m} \sum_{j=1}^{l} \left(d^i_{\mathcal{R}_1}(\delta_j) - d^i_{\mathcal{R}_2}(\delta_j)\right)^2 \times \max\left(c^i_F(\delta_j, \delta_d)\right)\right]^{\frac{1}{2}}. \quad (5)$$

Normalized plithogenic Euclidean distance (NPED) measure uses normalization including a factor of $1/n$ to address the dimensionality of the data set.

$$d^{\mathcal{R}}_{NE}(\mathcal{R}_1, \mathcal{R}_2) = \frac{1}{n}\left[\frac{1}{m} \sum_{i=1}^{m} \sum_{j=1}^{l} \left(d^i_{\mathcal{R}_1}(\delta_j) - d^i_{\mathcal{R}_2}(\delta_j)\right)^2 \times \max\left(c^i_F(\delta_j, \delta_d)\right)\right]^{\frac{1}{2}}. \quad (6)$$

In the above formulas, the term $\max(c^i_F(\delta_j, \delta_d))$ represents the maximal contradiction degree among elements of the PHSSs with respect to attributes δ_j and δ_d. This component reflects the highest level of uncertainty or conflict between the corresponding attributes in $\mathcal{R}_1$ and $\mathcal{R}_2$, thus significantly influencing the computation of distances. The selection of the maximal contradiction degree emphasizes the most significant disparities, enhancing the sensitivity of the distance measure to critical differences between the sets.

Definition 4. (*Hema* et al., *2023*) A newly proposed concept, termed the Pythagorean similarity measure (PSM), is aimed at the innovative development of the Pythagorean distance measure (PDM). This relationship is mathematically articulated as

$$\mathcal{M}^{\mathcal{R}}(\mathcal{R}_1, \mathcal{R}_2) = \frac{1}{1 + d^{\mathcal{R}}(\mathcal{R}_1, \mathcal{R}_2)}.$$

Algorithm 1.

Step 1. Read the registered input images I.

Step 2. To formalize the concept of an intuitionistic hypersoft set (IHSS), we delineate its construction based on the following components:

- *Membership degree construction*:
  The membership degree function for IHSS is

$$\mu_{I_1}^{\text{IHSS}} = \frac{I_{gh_1} - I_{\min}}{I_{\max} - I_{\min}}, \tag{7}$$

  where I_{gh_1} represents the gray level of a pixel in the first input image, and $I_{\max}$ and $I_{\min}$ denote the maximum and minimum gray level values in that image, respectively.

- *Non-membership function construction*:
  The non-membership function for the IHSS, is defined to complement the membership function and calculated as

$$\nu_{I_1}^{\text{IHSS}} = 1 - \mu_{I_1}^{\text{IHSS}}. \tag{8}$$

Step 3. Calculate the distance measure between two sets using Eqn. (1).

Step 4. Calculate the similarity measure using Eqn. (2).

Step 5. Select the one with the highest similarity measure as the optimal choice.

In this context, $d^{\mathcal{R}}(\mathcal{R}_1, \mathcal{R}_2)$ signifies the plithogenic distance. Notably, this distance is classified into several types, including: the plithogenic Hamming distance $d_H^{\mathcal{R}}(\mathcal{R}_1, \mathcal{R}_2)$, the normalized plithogenic Hamming distance $d_{NH}^{\mathcal{R}}(\mathcal{R}_1, \mathcal{R}_2)$, the plithogenic Euclidean distance $d_E^{\mathcal{R}}(\mathcal{R}_1, \mathcal{R}_2)$, or the normalized plithogenic Euclidean distance $d_{NE}^{\mathcal{R}}(\mathcal{R}_1, \mathcal{R}_2)$.

2.1. Methodology I.

2.1.1. Application I. In this particular application, our primary aim is the diagnosis of COVID-19 in specific patients by determining their infection status. To accomplish this, we initially acquire chest images of the patient. We acquire chest X-ray images of individuals under suspicious and confirm COVID-19 case from the Kaggle (Prashant, 2020) platform and apply the methodology detailed in Step 2 to transform these images into IHSS format. See Algorithm 1 for details.

For references, an IHSS representative of a confirmed COVID-19 case is pre-stored within the system. By employing a similarity assessment technique, we scrutinize the correlation between the patient's IHSS and the COVID-19 reference IHSS archived in our database. A significant resemblance between the two IHSS profiles indicates a probable COVID-19 infection, thereby classifying the individual as a potential COVID-19 case. To facilitate rapid diagnostics and enable local treatment of patients in a cost-effective manner, we propose the creation of software designed as an on-line tool. This tool would cater to a domain of discussion involving two individuals under suspicion, denoted as $\mathfrak{X} = \{\alpha_1, \alpha_2\}$. Here, the set of parameters $\eth_1, \eth_2$, and $\eth_3$ represents certain perceptible symptoms; specifically, $\eth_1 = \{\varkappa_1, \varkappa_2\}$ (fever, cough), $\eth_2 = \{\varkappa_3, \varkappa_4\}$ (fatigue, sore throat), and $\eth_3 = \{\varkappa_5, \varkappa_6\}$ (vomiting, headache). Additionally, we define the Cartesian product of these sets as $\mathfrak{G} = \eth_1 \times \eth_2 \times \eth_3$, yielding $\mathfrak{G} = \{\mathfrak{g}_1, \mathfrak{g}_2, \mathfrak{g}3, \cdots, \mathfrak{g}8\}$ where each $\mathfrak{g}_i$, $i \in \{1, 2, \ldots, 8\}$ represents a triple encapsulating various combinations of symptoms.

Fig. 1. Sample image of suspected COVID-19 from Kaggle (Prashant, 2020).

Stage 1. Data selection process. Following this, we construct two IHSS frameworks with the guidance of healthcare experts, specifically designed for individuals suspected of having COVID-19, as described below:

$$\begin{aligned}\Gamma_{\mathfrak{A}} = \Big\{ & (\mathfrak{g}_1, \{(\alpha_1, 0.7, 0.1), (\alpha_2, 0.6, 0.2)\}),\\ & (\mathfrak{g}_2, \{(\alpha_1, 0.2, 0.7), (\alpha_2, 0.4, 0.5)\}),\\ & (\mathfrak{g}_3, \{(\alpha_1, 0.2, 0.3), (\alpha_2, 0.5, 0.4)\}),\\ & (\mathfrak{g}_4, \{(\alpha_1, 0.1, 0.2), (\alpha_2, 0, 1)\}),\\ & (\mathfrak{g}_5, \{(\alpha_1, 0.5, 0.1), (\alpha_2, 0.1, 0.5)\}),\\ & (\mathfrak{g}_6, \{(\alpha_1, 0.5, 0.6), (\alpha_2, 0.2, 0.3)\}),\\ & (\mathfrak{g}_7, \{(\alpha_1, 0.1, 0.3), (\alpha_2, 0.7, 0.1)\}),\\ & (\mathfrak{g}_8, \{(\alpha_1, 0, 1), (\alpha_2, 0.7, 0.2)\}) \Big\}, \end{aligned} \tag{9}$$

$$\Lambda_{\mathfrak{B}} = \Big\{(\mathfrak{g}_1, \{(\alpha_1, 0.9, 0.1), (\alpha_2, 0.1, 0.9)\}), (\mathfrak{g}_2, \{(\alpha_1, 0, 1), (\alpha_2, 0.1, 0.6)\}), (\mathfrak{g}_3, \{(\alpha_1, 0.1, 0.4), (\alpha_2, 0.4, 0.5)\}), (\mathfrak{g}_4, \{(\alpha_1, 0, 1), (\alpha_2, 0.6, 0.5)\}), (\mathfrak{g}_5, \{(\alpha_1, 0.1, 0.9), (\alpha_2, 0.8, 0.2)\}), (\mathfrak{g}_6, \{(\alpha_1, 0.6, 0.2), (\alpha_2, 0.2, 0.6)\}), (\mathfrak{g}_7, \{(\alpha_1, 1, 0), (\alpha_2, 0.4, 0.2)\}), (\mathfrak{g}_8, \{(\alpha_1, 0.1, 0.5), (\alpha_2, 0.1, 0.5)\})\Big\}. \tag{10}$$

Stage 2. The system is described as follows, with another IHSS already included in the system as a reference point:

$$\Upsilon_{\mathfrak{C}} = \Big\{(\mathfrak{g}_1, \{(\alpha_1, 0.1, 0.4), (\alpha_2, 03, 0.5)\}), (\mathfrak{g}_2, \{(\alpha_1, 0.2, 0.4), (\alpha_2, 0.1, 0.6)\}), (\mathfrak{g}_3, \{(\alpha_1, 0.8, 0.1), (\alpha_2, 0.5, 0.2)\}), (\mathfrak{g}_4, \{(\alpha_1, 0.2, 0.1), (\alpha_2, 0.4, 0.3)\}), (\mathfrak{g}_5, \{(\alpha_1, 0.1, 0.2), (\alpha_2, 0, 1)\}), (\mathfrak{g}_6, \{(\alpha_1, 0.9, 0.1), (\alpha_2, 0.5, 0.1)\}), (\mathfrak{g}_7, \{(\alpha_1, 0.4, 0.5), (\alpha_2, 0.8, 0.1)\}), (\mathfrak{g}_8, \{(\alpha_1, 0.6, 0.3), (\alpha_2, 0.1, 0.7)\})\Big\}. \tag{11}$$

Stage 3. The Hamming distances from $\Gamma_{\mathfrak{A}}$ to $\Upsilon_{\mathfrak{C}}$ and from $\Lambda_{\mathfrak{B}}$ to $\Upsilon_{\mathfrak{C}}$ are approximately 0.55 and 0.57, respectively.

Stage 4. Results of the analysis.

(i) Computing the similarity measure between $\Gamma_{\mathfrak{A}}$ and $\Upsilon_{\mathfrak{C}}$:

$$S'_{\text{IHSS}}(\Gamma_{\mathfrak{A}}, \Upsilon_{\mathfrak{C}}) = \frac{1}{1 + d^s_{\text{IHSS}}(\Gamma_{\mathfrak{A}}, \Upsilon_{\mathfrak{C}})} \approx 0.6 > \frac{1}{2}.$$

(ii) Computing the similarity measure between $\Lambda_{\mathfrak{B}}$ and $\Upsilon_{\mathfrak{C}}$:

$$S'_{\text{IHSS}}(\Lambda_{\mathfrak{B}}, \Upsilon_{\mathfrak{C}}) = \frac{1}{1 + d^s_{\text{IHSS}}(\Lambda_{\mathfrak{B}}, \Upsilon_{\mathfrak{C}})} \approx 0.6 > \frac{1}{2}.$$

Stage 5. Therefore, both sets of symptoms $\Gamma_{\mathfrak{A}}$ and $\Upsilon_{\mathfrak{C}}$, as well as $\Lambda_{\mathfrak{B}}$ and $\Upsilon_{\mathfrak{C}}$, exhibit significant similarity. Consequently, it is inferred that the individual may potentially be afflicted with COVID-19.

Fig. 2. Sample image of suspected tuberculosis from Kaggle (Rahman, 2020).

2.1.2. Application II. Given the focus of our investigation, we identify a triple of subjects, denoted as $\mathfrak{X} = \{\alpha_1, \alpha_2, \alpha_3\}$, each under scrutiny for potential infection by tuberculosis (TB). We acquire chest X-ray images of individuals under suspicion and confirm a TB case from the Kaggle (Rahman, 2020) platform and apply the methodology detailed in Step 2 to transform these images into IHSS format.

The cornerstone of our approach is the diagnostic determination of infection presence among these individuals, leveraging the creation of patient-specific IHSS. We propose the development of unique IHSS models, $\mathfrak{I}_{\alpha_i}$, tailored to the distinctive medical profiles of each subject. These models will undergo comparative analysis against a predefined optimal TB IHSS model, $\mathfrak{I}_{\text{ideal}}$, housed within our database. This benchmark represents the quintessential immunological signature symptomatic of a TB infection. To quantitatively assess the proximity of each subject's IHSS to $\mathfrak{I}_{\text{ideal}}$, we employ a similarity measure. A measure exceeding a threshold of 0.5 will be indicative of a plausible TB infection, thus warranting further clinical investigation. Our analytical framework is further enriched by the delineation of symptomatic parameters across four distinct sets: $\mathfrak{S}_1, \mathfrak{S}_2, \mathfrak{S}_3$, and $\mathfrak{S}_4$. These sets encapsulate a range of observable symptoms, with $\mathfrak{S}_1 = \{\mathfrak{s}_1, \mathfrak{s}_2\}$, $\mathfrak{S}_2 = \{\mathfrak{s}_3, \mathfrak{s}_4\}$, $\mathfrak{S}_3 = \{\mathfrak{s}_5\}$, and $\mathfrak{S}_4 = \{\mathfrak{s}_6, \mathfrak{s}_7, \mathfrak{s}_8\}$. The symptoms are respectively identified as follows: $\mathfrak{s}_1$ for headache, $\mathfrak{s}_2$ for nausea and vomiting, $\mathfrak{s}_3$ for diarrhea, $\mathfrak{s}_4$ for abdominal pain, $\mathfrak{s}_5$ for chills, $\mathfrak{s}_6$ for cough, $\mathfrak{s}_7$ for muscle or joint pain, and $\mathfrak{s}_8$ for high fever. We define a relational set $\eta = \mathfrak{S}_1 \times \mathfrak{S}_2 \times \mathfrak{S}_3 \times \mathfrak{S}_4$, encompassing a collection of 4-tuples, $\eta = \{\eta_1, \eta_2, \ldots, \eta_{12}\}$, each η_i, where $i \in \{1, 2, \ldots, 12\}$, uniquely representing a combination of symptoms pertinent to our diagnostic evaluation.

Stage 1. Data selection process. Following this, we construct three IHSS frameworks with the guidance of healthcare experts, specifically designed for individuals with suspected TB.

$$\Gamma_{\mathfrak{A}} = \Big\{\{(\eta_1,\{(\alpha_1,0.3,0.5),(\alpha_2,0.3,0.2),(\alpha_3,0.1,0.5)\}),(\eta_2,\{(\alpha_1,0.2,0.4),(\alpha_2,0.1,0.1),(\alpha_3,0.5,0.4)\}),$$
$$(\eta_3,\{(\alpha_1,0.1,0.3),(\alpha_2,0.3,0.4),(\alpha_3,0.3,0.2)\}),(\eta_4,\{(\alpha_1,0.4,0.2),(\alpha_2,0,1),(\alpha_3,0.1,0.5)\}),$$
$$(\eta_5,\{(\alpha_1,0.1,0.3),(\alpha_2,0.4,0.5),(\alpha_3,0.1,0.2)\}),(\eta_6,\{(\alpha_1,0.1,0.7),(\alpha_2,0.2,0.3),(\alpha_3,0.1,0.6)\}),$$
$$(\eta_7,\{(\alpha_1,0.3,0.5),(\alpha_2,0.1,0.2),(\alpha_3,0,1)\}),(\eta_8,\{(\alpha_1,0.1,0.5),(\alpha_2,0.6,0.5),(\alpha_3,1,0)\}),$$
$$(\eta_9,\{(\alpha_1,0.3,0.2),(\alpha_2,0.1,0.3),(\alpha_3,0.1,0.7)\}),(\eta_{10},\{(\alpha_1,0.4,0.2),(\alpha_2,0.2,0.4),(\alpha_3,0.4,0.5)\}),$$
$$(\eta_{11},\{(\alpha_1,0.2,0.6),(\alpha_2,0.1,0.7),(\alpha_3,0.2,0.1)\}),(\eta_{12},\{(\alpha_1,0.1,0.1),(\alpha_2,0.4,0.3),(\alpha_3,0.1,0.3)\})\}\Big\}. \quad (12)$$

$$\Lambda_{\mathfrak{B}} = \Big\{\{(\eta_1,\{(\alpha_1,0.2,0.8),(\alpha_2,0.1,0.9),(\alpha_3,0.5,0.5)\}),(\eta_2,\{(\alpha_1,0.5,0.5),(\alpha_2,0.4,0.6),(\alpha_3,0.1,0.9)\}),$$
$$(\eta_3,\{(\alpha_1,0.6,0.4),(\alpha_2,0.3,0.7),(\alpha_3,0.8,0.2)\}),(\eta_4,\{(\alpha_1,0,1),(\alpha_2,0.5,0.5),(\alpha_3,1,0)\}),$$
$$(\eta_5,\{(\alpha_1,0.9,0.1),(\alpha_2,0.2,0.8),(\alpha_3,0.6,0.4)\}),(\eta_6,\{(\alpha_1,0.6,0.4),(\alpha_2,0.4,0.6),(\alpha_3,0.5,0.5)\}),$$
$$(\eta_7,\{(\alpha_1,0.5,0.5),(\alpha_2,0.6,0.4),(\alpha_3,0.9,0.1)\}),(\eta_8,\{(\alpha_1,0,1),(\alpha_2,0.9,0.1),(\alpha_3,0.1,0.9)\}),$$
$$(\eta_9,\{(\alpha_1,0.1,0.9),(\alpha_2,0.9,0.1),(\alpha_3,0.5,0.5)\}),(\eta_{10},\{(\alpha_1,0.9,0.1),(\alpha_2,0.2,0.8),(\alpha_3,0.8,0.2)\}),$$
$$(\eta_{11},\{(\alpha_1,0.5,0.5),(\alpha_2,0.3,0.7),(\alpha_3,0.5,0.5)\}),(\eta_{12},\{(\alpha_1,0.6,0.4),(\alpha_2,0.9,0.1),(\alpha_3,0.1,0.9)\})\}\Big\}. \quad (13)$$

$$\Upsilon_{\mathfrak{C}} = \Big\{\{(\eta_1,\{(\alpha_1,0.4,0.5),(\alpha_2,0.3,0.4),(\alpha_3,0.1,0.3)\}),(\eta_2,\{(\alpha_1,0.2,0.1),(\alpha_2,0.2,0.1),(\alpha_3,0.5,0.1)\}),$$
$$(\eta_3,\{(\alpha_1,0.1,0.4),(\alpha_2,0.6,0.3),(\alpha_3,0,1)\}),(\eta_4,\{(\alpha_1,1,0),(\alpha_2,0.5,0.4),(\alpha_3,1,0)\}),$$
$$(\eta_5,\{(\alpha_1,0.2,0.6),(\alpha_2,0.1,0.3),(\alpha_3,0.2,0.5)\}),(\eta_6,\{(\alpha_1,0.1,0.3),(\alpha_2,0.3,0.1),(\alpha_3,0,1)\}),$$
$$(\eta_7,\{(\alpha_1,0,1),(\alpha_2,0.2,0.4),(\alpha_3,1,0)\}),(\eta_8,\{(\alpha_1,0.6,0.5),(\alpha_2,0.2,0.3),(\alpha_3,0.4,0.5)\}),$$
$$(\eta_9,\{(\alpha_1,0.1,0.1),(\alpha_2,0.1,0.7),(\alpha_3,0.1,0.1)\}),(\eta_{10},\{(\alpha_1,0.3,0.6),(\alpha_2,0.2,0.2),(\alpha_3,1,0)\}),$$
$$(\eta_{11},\{(\alpha_1,0.1,0.5),(\alpha_2,0.1,0.3),(\alpha_3,0,1)\}),(\eta_{12},\{(\alpha_1,0.6,0.2),(\alpha_2,0.1,0.4),(\alpha_3,1,0)\})\}\Big\}. \quad (14)$$

Stage 2. The system is described by Eqns. (12)–(15), with another IHSS already included in the system as a reference point.

Stage 3. We evaluate the Hamming distances employing the IHSS metric, denoted by d^s_{IHSS}, between specific pairs of elements. Equation (1) can be used to calculate the distance between IHSSs, as specified below:

- Between $\Gamma_{\mathfrak{A}}$ and $\Psi_{\mathfrak{D}}$, the distance is $d^s_{\text{IHSS}}(\Gamma_{\mathfrak{A}},\Psi_{\mathfrak{D}}) = 0.7$.
- Between $\Lambda_{\mathfrak{B}}$ and $\Psi_{\mathfrak{D}}$, the distance is $d^s_{\text{IHSS}}(\Lambda_{\mathfrak{B}},\Psi_{\mathfrak{D}}) = 1.1$.
- Between $\Upsilon_{\mathfrak{C}}$ and $\Psi_{\mathfrak{D}}$, the distance is $d^s_{\text{IHSS}}(\Upsilon_{\mathfrak{C}},\Psi_{\mathfrak{D}}) = 0.9$.

Stage 4. Results of the analysis. Equation (2) can be used to calculate the SIM between IHSSs, as specified below:

- Compute the SIM of $\Gamma_{\mathfrak{A}}$ and $\Psi_{\mathfrak{D}}$:

$$S'_{\text{IHSS}}(\Gamma_{\mathfrak{A}},\Psi_{\mathfrak{D}}) = \frac{1}{1+d^s_{\text{IHSS}}(\Gamma_{\mathfrak{A}},\Psi_{\mathfrak{D}})} \cong 0.58 > \frac{1}{2}.$$

- Compute the SIM of $\Lambda_{\mathfrak{B}}$ and $\Psi_{\mathfrak{D}}$:

$$S'_{\text{IHSS}}(\Lambda_{\mathfrak{B}},\Psi_{\mathfrak{D}}) = \frac{1}{1+d^s_{\text{IHSS}}(\Lambda_{\mathfrak{B}},\Psi_{\mathfrak{D}})} \cong 0.4 < \frac{1}{2}.$$

- Compute the SIM of $\Upsilon_{\mathfrak{C}}$ and $\Psi_{\mathfrak{D}}$:

$$S'_{\text{IHSS}}(\Upsilon_{\mathfrak{C}},\Psi_{\mathfrak{D}}) = \frac{1}{1+d^s_{\text{IHSS}}(\Upsilon_{\mathfrak{C}},\Psi_{\mathfrak{D}})} \cong 0.52 > \frac{1}{2}.$$

Stage 5. From this information, it is likely that the

$$\Psi_{\mathfrak{D}} = \Big\{\{(\eta_1,\{(\alpha_1,0.1,0.5),(\alpha_2,0.6,0.4),(\alpha_3,0.5,0.5)\}),(\eta_2,\{(\alpha_1,0.6,0.1),(\alpha_2,0.8,0.2),(\alpha_3,0.9,0.1)\}),$$
$$(\eta_3,\{(\alpha_1,0.2,0.4),(\alpha_2,0.6,0.4),(\alpha_3,1,0)\}),(\eta_4,\{(\alpha_1,0.5,0.5),(\alpha_2,0.3,0.7),(\alpha_3,0.1,0.9)\}),$$
$$(\eta_5,\{(\alpha_1,0.7,0.1),(\alpha_2,0.8,0.2),(\alpha_3,0,1)\}),(\eta_6,\{(\alpha_1,0.2,0.8),(\alpha_2,0.1,0.9),(\alpha_3,0.5,0.5)\}),$$
$$(\eta_7,\{(\alpha_1,0.5,0.5),(\alpha_2,0,1),(\alpha_3,1,0)\}),(\eta_8,\{(\alpha_1,0.3,0.7),(\alpha_2,0.7,0.3),(\alpha_3,0.5,0.5)\}),$$
$$(\eta_9,\{(\alpha_1,0,1),(\alpha_2,0.6,0.4),(\alpha_3,0,1)\}),(\eta_{10},\{(\alpha_1,0.4,0.6),(\alpha_2,0.8,0.2),(\alpha_3,0.5,0.5)\}),$$
$$(\eta_{11},\{(\alpha_1,0.9,0.1),(\alpha_2,0.8,0.2),(\alpha_3,1,0)\}),(\eta_{12},\{(\alpha_1,0.1,0.9),(\alpha_2,0.4,0.6),(\alpha_3,0.5,0.5)\})\Big\}. \quad (15)$$

individuals α_1 and α_3 are affected by TB.

Remark 1. Note that on intuitionistic hypersoft set consists of two elements: membership values and non-membership values. In a medical context, the membership value indicates the degree to which a patient is healthy, expressed as a percentage. Conversely, the non-membership value represents the extent to which the patient is unhealthy, also expressed as a percentage. For instance, a value of (0.5, 0.3) implies that the patient is 50% healthy and 30% unhealthy. These percentages are determined through consultation with a medical professional.

2.2. Methodology II.

2.2.1. Algorithm.

Step 1. Read the registered input images I. To formalize the concept of an intuitionistic hypersoft set (IHSS), we delineate its construction based on the following components:

- *Membership degree construction*:

  The membership degree function for the IHSS is as follows:

$$\mu_{I_1}^{\text{IHSS}} = \frac{I_{gh_1} - I_{\min}}{I_{\max} - I_{\min}}, \quad (16)$$

  where I_{gh_1} represents the gray level of a pixel in the first input image, and $I_{\max}$ and $I_{\min}$ denote the maximum and minimum gray level values in that image, respectively.

- *Non-membership function construction*: The non-membership function for the IHSS is defined to complement the membership function and calculated as

$$\nu_{I_1}^{\text{IHSS}} = 1 - \mu_{I_1}^{\text{IHSS}}. \quad (17)$$

Step 2. Transform the IHSS into a fuzzy hypersoft set by applying the following formula:

$$\sigma_{\text{fuzzy}}(x) = \frac{1 - \mu_{I_1}^{\text{IHSS}}}{1 + (\mu_{I_1}^{\text{IHSS}} + \nu_{I_1}^{\text{IHSS}})}. \quad (18)$$

Step 3. To create a decision average matrix for each alternative based on the collective perspective of professionals in the IHSS, we utilize the standardized precipitation fuzzy conceptual framework. To apply the TOPSIS, we need to rank the efficiency of each option using

$$r_{ij} = \frac{x_{ij}}{\sqrt{\sum_{i=1}^{\mathrm{m}} x_{ij}^2}} \quad (19)$$

$i = 1, 2, \ldots, m$ and $j = 1, 2, \ldots, n$.

Step 4. Based on the weighted normalized rating (y_{ij}), the weighted normalized fuzzy control matrix is computed as follows:

$$y_{ij} = r_{ij} w_i, \quad (20)$$

$i = 1, 2, \ldots, m$ and $j = 1, 2, \ldots, n$.

Step 5. To get optimal positive and negative solutions, we formulate matrices for the positive ideal solution (PIS) and the negative ideal solution (NIS). The positive ideal solution matrix is derived through

$$A^+ = (y_1^+, y_2^+, y_3^+, \ldots, y_n^+), \quad (21)$$

while the negative ideal solution matrix is computed using

$$A^- = (y_1^-, y_2^-, y_3^-, \ldots, y_n^-). \quad (22)$$

Step 6. Compute the Euclidean distance of each alternative to the PIS and NIS. The distances are calculated using the following equations: for the distance of alternative A_i from the positive ideal solution

$$D_i^+ = \sqrt{\sum_{j=1}^{\mathrm{n}} (y_i^+ - y_{ij})^2}, \quad (23)$$

and for the distance of alternative A_i from the negative ideal solution

$$D_i^- = \sqrt{\sum_{j=1}^{n}(y_i^- - y_{ij})^2}. \tag{24}$$

Here, $i = 1, 2, \ldots, m$, and j are indexes for the criteria or attributes considered in the analysis. The symbols y_i^+ and y_i^- represent the values of the i-th alternative at the PIS and NIS, respectively, and y_{ij} represents the value of the i-th alternative on the j-th criterion.

Step 7. Calculate the preference value for each alternative involves determining the value of preference, denoted as V_i, for every option:

$$V_i = \frac{D_i^-}{D_i^- + D_i^+}, \tag{25}$$

where $i = 1, 2, \ldots, m$.

Step 8. Order the options according to their relative closeness values. The option with the highest relative closeness value is deemed the most favorable.

2.2.2. Numerical example. The main aim is to ascertain the most impactful infectious disease in North America. We define the ensemble $\mathfrak{X}$, which is constituted by the elements $\{\alpha_1, \alpha_2, \alpha_3, \alpha_4\}$:

- α_1 represents the TB disease,
- α_2 is indicative of Lyme disease,
- α_3 corresponds to ParaLyme disease,
- α_4 encapsulates Norovirus.

Each disease α_i for $i = 1, 2, 3, 4$ is associated with a collection of sub-parametric triplets denoted by $\mathfrak{H}_i$, which represent the symptomatic parameter values for that disease. Our goal, with the guidance of experts, is to discern which of these diseases exerts the most significant influence on the population. The methodology begins by collecting images from affected individuals.

Stage 1. Data selection process.

1. These images are then converted into IHSS format using Eqns. (16) and (17). The resulting IHSS data is presented in Table 1.
2. The step involves processing the IHSS data displayed in Table 1, converting it to fuzzy hypersoft set (FHSS) data as evidenced in Table 2, by Eqn. (18).
3. Following this, Table 2 is normalized to produce Table 3, as described by Eqn. (19).
4. Employing Eqn. (22), a weighted decision matrix is formulated for the options, as shown in Table 4.
5. The positive ideal solution and the negative ideal solution are determined by applying Eqns. (21) and (22), respectively, with the results displayed in Tables 5 and 6.
6. Calculate the Euclidean distances from each alternative to the PIS and NIS using Eqns. (23) and (24). The calculations are detailed in Tables 7 and 8.
7. Derive the preference value for each option using Eqn. (25), as detailed in Table 9.
8. Organize the options to determine the most significant one, indicating that TB disease has the greatest impact in this region, followed by the subsequent rankings as depicted in Table 10.

2.3. Methodology III.

2.3.1. Proposed algorithm. Consider a group, U, representing individuals who could be suspected infected with TB. Suppose that $\mathcal{R} = \{s_1, s_2, \ldots, s_k\} \subset U$ represents a subgroup comprising individuals currently being scrutinized. Let $\mathcal{Q} = \{\beta_1, \beta_2, \ldots, \beta_n\}, n \geq 1$, symbolize a collection of symptoms or attributes, and let $B = \{\beta_1, \beta_2, \ldots, \beta_m\}, m \leq n$, where $B \subset \mathcal{Q}$, represent a subset of these symptoms that are currently under analysis. The Cartesian product $C = A_1 \times A_2 \times \cdots \times A_n$ is formed, where A_i for $i = 1, 2, \ldots, n$ pertains to the set of possible outcomes for attribute β_i. It is crucial that these sets are exclusive of one another, ensuring $A_i \cap A_j = \emptyset$ for any $i, j \in \{1, 2, \ldots, n\}$.

For every individual s in $\mathcal{R}$, a relationship $d(s, \delta)$ is established, showcasing the degree of connection of s to each attribute value δ. This relationship is articulated in terms of fuzzy, intuitionistic fuzzy, or neutrosophic logic. The aim for medical practitioners is to leverage this model to gauge the probability of TB infection among the scrutinized individuals and ascertain the infection's intensity, thereby facilitating an informed decision-making process regarding each case. The subsequent sections will elaborate on the AI-based methodology employed in developing this algorithm for such assessments.

2.4. Implementation of the proposed method. Consider a defined universe U and within it, a subset $\mathcal{R} = \{s_1, s_2, \ldots, s_5\}$ that includes individuals suspected of being infected with TB.

Stage 1. Data selection process.

Table 1. All experts' opinions collectively (IHSS values).

Types of diseases	$\mathfrak{H}_1$	$\mathfrak{H}_2$	$\mathfrak{H}_3$	$\mathfrak{H}_4$
TB disease	(0.4, 0.5)	(0.3, 0.1)	(0.3, 0.2)	(0.4, 0.3)
Lyme disease	(0.8, 0.1)	(0.7, 0)	(0.9, 0)	(0.5, 0.3)
ParaLyme disease	(0.2, 0.2)	(0.5, 0.1)	(0.8, 0.1)	(0.4, 0.2)
Norovirus	(0.1, 0.1)	(0.4, 0.3)	(0.1, 0.2)	(0.6, 0.3)

Table 2. All experts' opinions collectively (FHS values).

Types of diseases	$\mathfrak{H}_1$	$\mathfrak{H}_2$	$\mathfrak{H}_3$	$\mathfrak{H}_4$
TB disease	0.31	0.5	0.46	0.35
Lyme disease	0.11	0.17	0.05	0.27
ParaLyme disease	0.57	0.31	0.11	0.37
Norovirus	0.75	0.35	0.79	0.21

Step 1. The assessment of these individuals is based on monitoring various symptoms or attributes, listed as follows:

$$\begin{aligned}
\beta_1 &= \text{fever},\\
\beta_2 &= \text{dry cough},\\
\beta_3 &= \text{tiredness},\\
\beta_4 &= \text{breathing difficulty or breath shortness},\\
\beta_5 &= \text{chest pain or pressure},\\
\beta_6 &= \text{loss of speech or movement},\\
\beta_7 &= \text{aches and pains},\\
\beta_8 &= \text{throat discomfort},\\
\beta_9 &= \text{diarrhea},\\
\beta_{10} &= \text{conjunctivitis},\\
\beta_{11} &= \text{headache},\\
\beta_{12} &= \text{diminished ability to taste or smell},\\
\beta_{13} &= \text{skin rash or changes in the color of}\\
&\qquad \text{the fingers or toes.}
\end{aligned}$$

To better gauge the intensity of these symptoms in the suspects, each symptom, denoted as β_i, is classified into three severity tiers: low (L) for mild symptoms, medium (M) for moderate symptoms, and high (H) for severe symptoms. This classification aids in enhancing the diagnostic process by allocating specific severity levels:

$$\begin{aligned}
\delta(i,1) &= \text{low},\\
\delta(i,2) &= \text{medium},\\
\delta(i,3) &= \text{high},
\end{aligned}$$

for $1 \leq i \leq 13$. The subset of symptoms that are observed in suspects from a particular area includes $\beta_1, \beta_2, \beta_3, \beta_4, \beta_5, \beta_6, \beta_9, \beta_{11}$. To each suspect, a hypothetical fuzzy membership degree is assigned for each chosen symptom, under specific constraints defined by experts, to validate the approach. For this, see Table 11.

Step 2. For each symptom selected, a predominant attribute value δ_d and a fuzzy contradiction degree c_F reflecting the discrepancy between the actual and the predominant attribute values are identified in Table 12.

A PHSS $\mathcal{R}_1$ has been developed and its data are organized in a table format, incorporating the insights from a specialist field expert doctor, as depicted in Table 13. The values for the selected symptoms determined by the experts are also detailed in Table 14.

Step 3. To assess the discrepancy between specialist-recorded values and established benchmarks, the study employs plithogenic Hamming and Euclidean distances as delineated in Eqns. (26) and (27), with findings presented in Table 15. Following this, the investigation evaluates plithogenic similarity, leveraging plithogenic distance, to gauge the extent of infection in the observed subjects.

Step 4. Now, plithogenic similarity, derived from plithogenic distance, is assessed to evaluate the degree of infection in the suspects being observed, as noted in Table 16. The values for both Hamming and Euclidean similarity measures are efficiently retrieved from Table 16.

Steps 5 and 6. These values inform the subsequent decisions made regarding the suspects, which are detailed in Table 17. Figure 3 provides a graphical depiction of the suspects.

2.4.1. Limitations. The described approach has certain limitations, including the following:

(i) Limited data quality and accessibility may hinder model accuracy.

(ii) AI model biases may impair generalization across diverse populations.

(iii) The complexity of AI algorithms raises interpretability and ethical issues.

Table 3. Normalized matrix.

Types of diseases	$\mathfrak{H}_1$	$\mathfrak{H}_2$	$\mathfrak{H}_3$	$\mathfrak{H}_4$
TB disease	0.31068	0.70888	0.5489	0.57048
Lyme disease	0.11024	0.24102	0.05966	0.44009
ParaLyme disease	0.57126	0.43951	0.13126	0.60308
Norovirus	0.75166	0.49622	0.82336	0.34229

Table 4. Weighted normalized matrix.

Types of diseases	$\mathfrak{H}_1$	$\mathfrak{H}_2$	$\mathfrak{H}_3$	$\mathfrak{H}_4$
TB disease	0.03107	0.28355	0.10978	0.1141
Lyme disease	0.01102	0.09641	0.01193	0.08802
ParaLyme disease	0.05713	0.1758	0.022625	0.12062
Norovirus	0.07517	0.19849	0.16467	0.06846

Table 5. Positive ideal solution.

Types of diseases	Ideal positive values
$\mathfrak{C}_1$	0.01102
$\mathfrak{C}_2$	0.09641
$\mathfrak{C}_3$	0.01193
$\mathfrak{C}_4$	0.06846

Table 6. Negative ideal solution.

Types of diseases	Ideal negative values
$\mathfrak{C}_1$	0.07517
$\mathfrak{C}_2$	0.28355
$\mathfrak{C}_3$	0.16467
$\mathfrak{C}_4$	0.12062

Table 7. Euclidean distance from ideal positive.

Types of diseases	Separation values
TB disease	0.21698
Lyme disease	0.01956
ParaLyme disease	0.10656
Norovirus	0.19458

Table 8. Euclidean distance from ideal negative.

Types of diseases	Separation values
TB disease	0.07071
Lyme disease	0.25205
ParaLyme disease	0.17634
Norovirus	0.09978

2.4.2. Comparative studies. We investigated the efficacy and superiority of our suggested similarity metrics and TOPSIS-driven methodologies, incorporated within the hybrid framework of hypersoft sets, through various comparative analyses. These assessments shed light on both the advantages and limitations of our approaches when compared with already established methodologies. The evaluation entailed juxtaposing our approach with a variety of existing techniques within the field. One significant drawback of current methodologies is their inability to effectively handle the division of attributes into attribute values, especially when dealing with complex uncertain data. Our methods adeptly address these crucial challenges, setting themselves apart from the deficiencies inherent in established methodologies. For a more comprehensive understanding, consult Table 18.

3. Conclusion

This study contributes significantly to the field of medical diagnostics through the development and application of three advanced AI-based approaches using image analysis to enhance disease diagnosis accuracy. These methodologies not only provide a systematic solution but also represent an innovative integration of computational techniques with multi-criteria decision-making frameworks, specifically tailored to address the challenges in diagnosing diseases like COVID-19. Firstly, the intuitionistic hypersoft set (IHSS) approach leverages distance and similarity measures to effectively transform and analyze medical images, enhancing diagnostic accuracy by incorporating uncertainty and imprecision inherent in medical data. Secondly, the application of the TOPSIS method demonstrates a robust framework for ranking and selecting the best diagnostic outcomes based on a set of predefined criteria, facilitating better clinical decisions. Lastly, the adoption of plithogenic distance and similarity measures in plithogenic hypersoft sets offers a novel perspective in decision-making processes, particularly in assessing the severity of COVID-19 infections, which is crucial for timely and appropriate medical interventions.

Despite these advancements, the study does encounter limitations that could serve as focal points for future research. For instance, the specific datasets

Table 9. Preference values.

Types of diseases	Values
TB disease	0.24578
Lyme disease	0.92799
ParaLyme disease	0.62333
Norovirus	0.33897

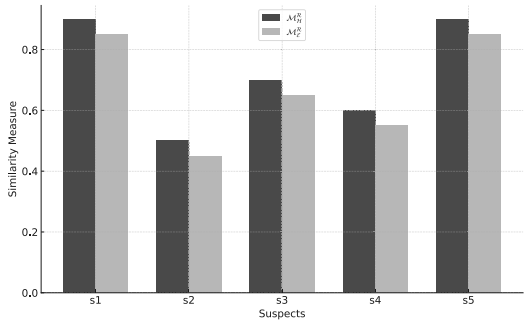

Fig. 3. Similarity among suspects in a plithogenic context.

used, derived from the Kaggle platform, may not comprehensively represent the global variability in COVID-19 manifestations. Further investigations could explore the adaptability of these methodologies to other datasets or even to other diseases, potentially broadening the applicability of the findings. Additionally, the complex mathematical models and computational intensity of these methods may limit their immediate application in resource-limited settings, highlighting the need for more scalable and accessible diagnostic solutions.

In the future, the study will increasingly concentrate on refining AI algorithms to boost their precision, efficiency, and reliability in diagnosing a wider array of infectious diseases using various imaging techniques. The integration of these AI solutions with real-time data analytics and wearable health technologies is expected to enable early detection and tailored treatment plans. Moreover, the development of federated learning models will allow these AI systems to learn from extensive, decentralized data sets while safeguarding patient privacy, thus enhancing diagnostic performance without jeopardizing data security. Collaborations across disciplines, including machine learning, bioinformatics, virology, and clinical medicine, are deemed essential for addressing current challenges and broadening the reach of these diagnostic tools to under-resourced areas.

Algorithm 2. Diagnostic algorithm.

Step 1. In the PHSS $\mathcal{R}_1$, the specialist assigns a fuzzy membership degree to each suspect in relation to each symptom.

Step 2. Organize the disease symptoms under investigation into a set based on their established values, grouping them according to sub-symptoms and categorizing each by severity, as denoted by PHSS $\mathcal{R}_2$.

Step 3. Utilizing the newly proposed distance measures, namely the PHD measure and the PED measure, evaluate the distance between the PHSS $\mathcal{R}1$ and $\mathcal{R}2$, as described below:

$$d_H^{\mathcal{R}}(\mathcal{R}_1,\mathcal{R}_2)=\frac{1}{m}\sum_{i=1}^{m}\sum_{j=1}^{l}\left|d^i_{\mathcal{R}_1}(\delta_j)-d^i_{\mathcal{R}_2}(\delta_j)\right| \times\max\left(c^i_F(\delta_j,\delta_d)\right), \tag{26}$$

$$d_E^{\mathcal{R}}(\mathcal{R}_1,\mathcal{R}_2)=\Big[\frac{1}{m}\sum_{i=1}^{m}\sum_{j=1}^{l}\left(d^i_{\mathcal{R}_1}(\delta_j)-d^i_{\mathcal{R}_2}(\delta_j)\right)^2 \times\max\left(c^i_F(\delta_j,\delta_d)\right)\Big]^{\frac{1}{2}}, \tag{27}$$

where m denotes the count of selected attributes and l indicates the number of values for each attribute.

Step 4. Calculate the plithogenic similarity measure (PSM) by first determining the distance plithogenic distance measure (PDM) between values assigned by experts and the corresponding standard values to evaluate their resemblance

$$\mathcal{M}^{\mathcal{R}}=\mathcal{M}^{\mathcal{R}}(\mathcal{R}_1,\mathcal{R}_2)=\frac{1}{1+d^{\mathcal{R}}(\mathcal{R}_1,\mathcal{R}_2)}. \tag{28}$$

The PSM determines the similarity between two PHSS, $\mathcal{R}1$ and $\mathcal{R}2$, to be plithogenically similar if $S^{\mathcal{R}} \geq 0.5$. This threshold value of 0.5 indicates similarity but may vary for normalized plithogenic distances. Here, $d^{\mathcal{R}}(\mathcal{R}1,\mathcal{R}2)$ represents any plithogenic distance within the framework of the proposed PDM.

Step 5. If the suspect is not infected, then it is indicated by $\mathcal{M}^{\mathcal{R}}$ being less than 0.5.

Step 6. If the metric $\mathcal{M}^{\mathcal{R}}$ meets or exceeds the threshold of 0.5, this serves as an indication that the individual in question may be infected. Following this assessment, subsequent actions will be determined by evaluating the level of infection severity:

- If the suspect's $\mathcal{M}^{\mathcal{R}}$ value is between 0.5 and 0.7, they must be isolated and quarantined at home appropriately.
- If the suspect's $\mathcal{M}^{\mathcal{R}}$ value is between 0.7 and 0.9 (inclusive of 0.7 but exclusive of 0.9), they must be isolated in a designated quarantine facility.
- If the measure $\mathcal{M}^{\mathcal{R}}$ falls within the range of 0.9 to 1, it is mandatory to dispatch the suspect to the hospital for appropriate medical care.

Table 10. Final ranking matrix.

Types of diseases	$\mathfrak{H}_1$	$\mathfrak{H}_2$	$\mathfrak{H}_3$	$\mathfrak{H}_4$	Rank
TB disease	0.31	0.5	0.46	0.35	1
Lyme disease	0.11	0.17	0.05	0.27	4
ParaLyme disease	0.57	0.31	0.11	0.37	3
Norovirus	0.75	0.35	0.79	0.21	2

Table 11. Degree of belongingness of each option with respect to each attribute value, measured in fuzzy terms.

Symptoms	Severity	Suspects				
		s_1	s_2	s_3	s_4	s_5
β_1	Low	0.64	0.43	0.25	0.49	0.19
	Medium	0.81	0.54	0.24	0.52	0.36
	High	0.97	0.76	0.40	0.67	0.21
β_2	Low	0.51	0.52	0.45	0.39	0.23
	Medium	0.57	0.64	0.49	0.52	0.34
	High	0.74	0.75	0.29	0.67	0.56
β_3	Low	0.54	0.61	0.21	0.28	0.43
	Medium	0.65	0.31	0.36	0.61	0.56
	High	0.81	0.45	0.35	0.65	0.67
β_4	Low	0.47	0.41	0.27	0.54	0.23
	Medium	0.58	0.42	0.61	0.68	0.31
	High	0.59	0.56	0.70	0.63	0.38
β_5	Low	0.56	0.41	0.20	0.51	0.56
	Medium	0.58	0.42	0.19	0.67	0.58
	High	0.81	0.45	0.32	0.76	0.59
β_6	Low	0.65	0.45	0.41	0.60	0.23
	Medium	0.67	0.49	0.42	0.82	0.34
	High	0.78	0.78	0.49	0.73	0.56
β_7	Low	0.45	0.13	0.15	0.21	0.23
	Medium	0.48	0.23	0.23	0.38	0.27
	High	0.49	0.29	0.34	0.39	0.29
β_8	Low	0.21	0.29	0.19	0.19	0.22
	Medium	0.34	0.29	0.37	0.39	0.31
	High	0.29	0.49	0.61	0.29	0.39
β_9	Low	0.54	0.67	0.65	0.43	0.46
	Medium	0.62	0.65	0.80	0.56	0.51
	High	0.61	0.87	0.18	0.51	0.58
β_{10}	Low	0.23	0.24	0.21	0.26	0.26
	Medium	0.31	0.21	0.24	0.43	0.34
	High	0.45	0.43	0.45	0.45	0.47
β_{11}	Low	0.65	0.65	0.54	0.29	0.25
	Medium	0.72	0.67	0.56	0.49	0.36
	High	0.76	0.70	0.67	0.59	0.47
β_{12}	Low	0.21	0.23	0.14	0.23	0.13
	Medium	0.34	0.45	0.23	0.28	0.24
	High	0.43	0.52	0.39	0.21	0.36
β_{13}	Low	0.35	0.32	0.35	0.24	0.25
	Medium	0.37	0.45	0.45	0.26	0.29
	High	0.45	0.54	0.48	0.27	0.29

Table 12. Degrees of contradiction correlating with the dominant value.

Symptoms	Dominant	L	M	H
β_1	High	0.82	0.670	0.00
β_2	High	0.99	0.58	0.00
β_3	Medium	0.31	0.00	0.58
β_4	High	0.98	0.82	0.00
β_5	High	0.97	0.81	0.00
β_6	Medium	0.46	0.00	0.52
β_9	Low	0.00	0.42	0.89
β_{11}	Low	0.00	0.45	0.88

Table 13. Degree of affiliation assigned to the suspects by the specialist using fuzzy logic.

Symptoms	Severity	Suspects				
		s_1	s_2	s_3	s_4	s_5
β_1	Low	0.64	0.43	0.25	0.49	0.19
	Medium	0.81	0.54	0.24	0.61	0.36
	High	0.97	0.76	0.40	0.76	0.19
β_2	Low	0.51	0.52	0.45	0.39	0.23
	Medium	0.57	0.64	0.49	0.52	0.34
	High	0.74	0.75	0.29	0.67	0.56
β_3	Low	0.54	0.61	0.21	0.28	0.43
	Medium	0.65	0.31	0.36	0.61	0.56
	High	0.81	0.45	0.35	0.61	0.67
β_4	Low	0.47	0.41	0.31	0.54	0.23
	Medium	0.58	0.42	0.61	0.70	0.31
	High	0.59	0.56	0.68	0.67	0.38
β_5	Low	0.56	0.41	0.21	0.51	0.56
	Medium	0.58	0.42	0.19	0.67	0.58
	High	0.81	0.45	0.29	0.76	0.59
β_6	Low	0.65	0.45	0.41	0.61	0.23
	Medium	0.67	0.49	0.42	0.79	0.34
	High	0.78	0.78	0.49	0.69	0.56
β_9	Low	0.54	0.67	0.65	0.43	0.46
	Medium	0.62	0.65	0.80	0.56	0.51
	High	0.61	0.87	0.18	0.51	0.58
β_{11}	Low	0.65	0.65	0.54	0.33	0.25
	Medium	0.72	0.67	0.56	0.55	0.36
	High	0.76	0.70	0.67	0.60	0.47
β_{12}	Low	0.21	0.23	0.14	0.23	0.13
	Medium	0.34	0.41	0.23	0.28	0.24
	High	0.43	0.52	0.39	0.21	0.36
β_{13}	Low	0.35	0.32	0.35	0.24	0.25
	Medium	0.37	0.45	0.45	0.26	0.29
	High	0.45	0.54	0.48	0.27	0.29

Acknowledgment

This paper has received funding from the Research Council of Lithuania through the project *Bridging Medical Imaging and Explainable Machine Learning: Algorithms for Precise Diagnostics* (no. S-PD-24-12).

References

Atanassov, K.T. (2012). *On Intuitionistic Fuzzy Sets Theory*, Springer, Heidelberg.

Chaira, T. (2011). Intuitionistic fuzzy set theory in medical imaging, *International Journal of Soft Computing and En-*

Table 14. Established criteria for selected symptoms.

Attributes	Low	Medium	High
β_1	0.60	0.74	0.97
β_2	0.60	0.76	0.87
β_3	0.70	0.76	0.81
β_4	0.69	0.81	0.99
β_5	0.68	0.82	0.98
β_6	0.78	0.91	1.00
β_9	0.39	0.61	0.69
β_{11}	0.39	0.65	0.71

Table 15. Distance measures.

Suspects	$d_H^{\mathcal{R}}(\mathcal{R}_1, \mathcal{R}_2)$	$d_E^{\mathcal{R}}(\mathcal{R}_1, \mathcal{R}_2)$
s_1	0.081	0.083
s_2	0.32	0.31
s_3	1.23	1.19
s_4	0.44	0.53
s_5	1.4	1.5

Table 16. Similarity measures.

Suspects	$\mathcal{M}_H^{\mathcal{R}}(\mathcal{R}_1, \mathcal{R}_2)$	$\mathcal{M}_E^{\mathcal{R}}(\mathcal{R}_1, \mathcal{R}_2)$
s_1	0.89	0.88
s_2	0.53	0.48
s_3	0.81	0.83
s_4	0.72	0.67
s_5	0.92	0.91

Table 17. Suspects decision.

Similarity index	Decision	Suspects
$0 \leq \mathcal{M}^p < 0.45$	Safe zone	s_3
$0.45 \leq \mathcal{M}^{\mathcal{R}} < 0.6$	Home isolation	s_2
$0.6 \leq \mathcal{M}^p < 0.8$	Quarantine center	s_4
$0.8 \leq \mathcal{M}^p \leq 1$	Hospital treatment	s_1, s_5

gineering **1**(2): 24–26.

Chin, C.-L., Lin, J.-C., Li, C.-Y., Sun, T.-Y., Chen, T., Lai, Y.-M., Huang, P.-C., Chang, S.-W. and Sharma, A.K. (2023). A novel fuzzy DBnet for medical image segmentation, *Electronics* **12**(12): 2658.

Curtis, C., Liu, C., Bollerman, T.J. and Pianykh, O.S. (2018). Machine learning for predicting patient wait times and appointment delays, *Journal of the American College of Radiology* **15**(9): 1310–1316.

Davenport, T.H., Hongsermeier, T. and Mc Cord, K.A. (2018). Using AI to improve electronic health records, *Harvard Business Review* **12**(2): 1–6.

Dey, N., Ashour, A.S., Shi, F. and Balas, V.E. (2018). *Soft Computing Based Medical Image Analysis*, Academic Press, London.

Fauci, A.S. and Morens, D.M. (2012). The perpetual challenge of infectious diseases, *New England Journal of Medicine* **366**(5): 454–461.

Hasan, M.R., Ray, R.K. and Chowdhury, F.R. (2024). Employee performance prediction: An integrated approach of business analytics and machine learning, *Journal of Business and Management Studies* **6**(1): 215–219.

Hema, R., Sudharani, R. and Kavitha, M. (2023). A novel approach on plithogenic interval valued neutrosophic hyper-soft sets and its application in decision making, *Indian Journal of Science and Technology* **16**(32): 2494–2502.

Jiang, Y., Tang, Y. and Chen, Q. (2011). An adjustable approach to intuitionistic fuzzy soft sets based decision making, *Applied Mathematical Modelling* **35**(2): 824–836.

Kamacı, H. (2021). On hybrid structures of hypersoft sets and rough sets *International Journal of Modern Science and Technology* **6**(4): 69–82.

Kaur, P. and Chaira, T. (2021). A novel fuzzy approach for segmenting medical images, *Soft Computing* **25**(5): 3565–3575.

Koundal, D. and Sharma, B. (2019). Challenges and future directions in neutrosophic set-based medical image analysis, *in* Y. Guo and A.S. Ashour (Eds), *Neutrosophic Set in Medical Image Analysis*, Elsevier, Amsterdam, pp. 313–343.

Lauraitis, A., Maskeliūnas, R. and Damaševičius, R. (2018). Ann and fuzzy logic based model to evaluate Huntington disease symptoms, *Journal of Healthcare Engineering* **2018**(1): 1–10.

Lin, D. and Lin, H. (2020). Translating artificial intelligence into clinical practice, *Annals of Translational Medicine* **8**(11): 715–715.

Lourenço-Silva, J. and Oliveira, A.L. (2021). Using soft labels to model uncertainty in medical image segmentation, *International MICCAI Brainlesion Workshop, Brno, Czech Republic*, pp. 585–596.

Morse, S.S. (1995). Factors in the emergence of infectious disease, *Emerging Infectious Diseases* **1**(1): 7–15.

Mumuni, A.N., Hasford, F., Udeme, N.I., Dada, M.O. and Awojoyogbe, B.O. (2024). A SWOT analysis of artificial intelligence in diagnostic imaging in the developing world: making a case for a paradigm shift, *Physical Sciences Reviews* **9**(1): 443–476.

Nagaraja Kumar, N., Jayachandra Prasad, T. and Satya Prasad, K. (2023). Multimodal medical image fusion with improved multi-objective meta-heuristic algorithm with fuzzy entropy, *Journal of Information & Knowledge Management* **22**(01): 2250063.

Omoregbe, N.A., Ndaman, I.O., Misra, S., Abayomi-Alli, O.O., Damaševičius, R. and Dogra, A. (2020). Text messaging-based medical diagnosis using natural language processing and fuzzy logic, *Journal of Healthcare Engineering* **2020**(1): 1–14.

Palanisami, D., Mohan, N. and Ganeshkumar, L. (2022). A new approach of multi-modal medical image fusion using intuitionistic fuzzy set, *Biomedical Signal Processing and Control* **77**(2): 103762.

Table 18. Comparative analysis.

References	Parameters	Sub-parameters	Membership	Falsity components	Ranking
Chaira (2011)	✓	×	✓	✓	×
Koundal and Sharma (2019)	✓	×	✓	✓	×
Kaur and Chaira (2021)	×	×	✓	×	×
Dey *et al*. (2018)	✓	×	×	×	×
Omoregbe *et al*. (2020)	×	×	✓	×	×
Lauraitis *et al*. (2018)	×	×	✓	×	×
Jiang *et al*. (2011)	✓	×	✓	✓	×
Lourenço-Silva and Oliveira (2021)	✓	×	×	×	×
Palanisami *et al*. (2022)	✓	×	✓	✓	×
Proposed method	✓	✓	✓	✓	✓

Prashant (2020). Chest X-ray COVID19 pneumonia dataset, https://www.kaggle.com/datasets/prashant268/chest-xray-covid19-pneumonia.

Rahman, T. (2020). Tuberculosis (TB) chest X-ray dataset, https://www.kaggle.com/datasets/tawsifurrahman/tuberculosis-tb-chest-xray-dataset.

Ramu, B. and Bansal, S. (2024). Highly accurate tumour region segmentation from magnetic resonance images using customized convolutional neural networks, *Multimedia Tools and Applications* **83**(5): 14423–14445.

Ray, R.K., Chowdhury, F.R. and Hasan, M.R. (2024). Blockchain applications in retail cybersecurity: Enhancing supply chain integrity, secure transactions, and data protection, *Journal of Business and Management Studies* **6**(1): 206–214.

Sundus, H., Khan, S.A., Chhabra, C., Jain, S., Aziz, R. and Kaur, H. (2024). Artificial intelligence and medical research: Accelerating innovation in healthcare, *in* S.A. Bansal and C. Chhabra (Eds), *AI Horizons: Exploring Multidisciplinary Frutiers*, Vol. III, Redshine Publication, Lahore, pp. 105–123.

Vemuri, N., Thaneeru, N. and Tatikonda, V.M. (2023a). Securing trust: Ethical considerations in AI for cybersecurity, *Journal of Knowledge Learning and Science Technology* **2**(2): 167–175.

Vemuri, N., Thaneeru, N. and Tatikonda, V.M. (2023b). Smart farming revolution: Harnessing IoT for enhanced agricultural yield and sustainability, *Journal of Knowledge Learning and Science Technology* **2**(2): 143–148.

Vemuri, N.V.N. (2023). Enhancing human-robot collaboration in industry 4.0 with AI-driven HRI, *Power System Technology* **47**(4): 341–358.

Zadeh, L.A. (1965). Fuzzy sets, *Information and Control* **8**(3): 338–353.

Yolcu, A., (2023). Intuitionistic fuzzy hypersoft topology and its applications to multi-criteria decision-making, *Sigma Journal of Engineering and Natural Sciences* **41**(1): 106–118.

Muhammad Ahsan received his PhD from the University of Management and Technology, Pakistan. He has authored 17 articles and two book chapters, focusing on decision-making, medical diagnosis, and machine learning.

Robertas Damaševičius is a professor at Vytautas Magnus University, specializing in e-health and assisted living technologies. He has an extensive publication record, having authored more than 640 papers and collaborated with over 750 co-authors. His contributions to the field have been recognized globally, with Stanford University ranking him in the World's Top 2% of world scientists.

Sarmad Shahzad holds a BS degree from Riphah International University in Pakistan, specializing in fuzzy medical diagnosis and decision-making.

Received: 17 March 2024
Revised: 29 April 2024
Accepted: 23 August 2024